Journal of Hydraulic Research Vol. 46, No. 3 (2008), pp. 373–381
doi:10.3826/jhr.2008.2848

Parameters affecting water-hammer wave attenuation, shape and timing—Part 1: Mathematical tools

Paramètres affectant l'atténuation, la forme et le retard du coup de bélier—Partie 1: Modèles mathématiques

ANTON BERGANT, (IAHR Member), *Litostroj E.I. d.o.o., 1000 Ljubljana, Slovenia. Tel.: +386 1 5824 284; fax: +386 1 5824 174; e-mail: anton.bergant@litostroj-ei.si (author for correspondence)*

ARRIS S. TIJSSELING, *Eindhoven University of Technology, P.O. Box 513, 5600 MB Eindhoven, The Netherlands. Tel.: +31 40 247 2755; fax: +31 40 244 2489; e-mail: a.s.tijsseling@tue.nl*

JOHN P. VÍTKOVSKÝ, (IAHR Member), *Department of Natural Resources and Water, Indooroopilly QLD 4068, Australia. Tel.: +61 7 3896 9134; fax: +61 7 3896 9898; e-mail: john.vitkovsky@nrw.qld.gov.au*

DÍDIA I.C. COVAS, *Instituto Superior Técnico, 1049-001 Lisboa, Portugal. Tel.: +351 21 8418 152; fax: +351 21 8418 150; e-mail: didia.covas@civil.ist.utl.pt*

ANGUS R. SIMPSON, (IAHR Member), *The University of Adelaide, Adelaide SA 5005, Australia. Tel.: +61 8 8303 5874; fax: +61 8 8303 4359; e-mail: asimpson@civeng.adelaide.edu.au*

MARTIN F. LAMBERT, (IAHR Member), *The University of Adelaide, Adelaide SA 5005, Australia. Tel.: +61 8 8303 5838; fax: +61 8 8303 4359; e-mail: mlambert@civeng.adelaide.edu.au*

ABSTRACT
This two-part paper investigates key parameters that may affect the pressure waveform predicted by the classical theory of water-hammer. Shortcomings in the prediction of pressure wave attenuation, shape and timing originate from violation of assumptions made in the derivation of the classical water-hammer equations. Possible mechanisms that may significantly affect pressure waveforms include unsteady friction, cavitation (including column separation and trapped air pockets), a number of fluid–structure interaction (FSI) effects, viscoelastic behaviour of the pipe-wall material, leakages and blockages. Engineers should be able to identify and evaluate the influence of these mechanisms, because first these are usually not included in standard water-hammer software packages and second these are often "hidden" in practical systems. Part 1 of the two-part paper describes mathematical tools for modelling the aforementioned mechanisms. The method of characteristics transformation of the classical water-hammer equations is used herein as the basic solution tool. In separate additions: a convolution-based unsteady friction model is explicitly incorporated; discrete vapour and gas cavity models allow cavities to form at computational sections; coupled extended water-hammer and steel-hammer equations describe FSI; viscoelastic behaviour of the pipe-wall material is governed by a generalised Kelvin–Voigt model; and blockages and leakages are modelled as end or internal boundary conditions.

RÉSUMÉ
Cet article, publié en deux parties, étudie les paramètres clés qui ne sont pas considérés par la théorie classique du coup de bélier et qui peuvent cependant avoir un effet significatif sur la forme de l'onde de pression. Les différences entre les valeurs calculées et observées dans l'atténuation, la forme et le retard de l'onde de pression sont expliquées par ces paramètres. Les ingénieurs devraient être capables d'identifier et évaluer l'influence de ces phénomènes puisque, tout d'abord, ils ne sont généralement pas considérés dans les logiciels commerciaux de calcul du coup de bélier, et, ensuite, ils se manifestent, souvent sous forme "masquée", dans les systèmes réels. Ces phénomènes sont notamment la friction transitoire, la cavitation (y compris la séparation de la colonne et les poches d'air), l'interaction de fluide structure (FSI), le comportement viscoélastique du matériel de la conduite, les fuites et les blocages. La première partie décrit les modèles mathématiques nécessaires pour calculer les effets de ces phénomènes. La méthode de caractéristiques (MOC) est utilisée comme outil base pour la transformation des équations classiques du coup de bélier. Le modèle pour le calcul de la friction transitoire, basé sur l'opération de circonvolution, y est explicitement incorporé. Les modèles discrets de cavité de vapeur et de gaz permettent de simuler la cavitation aux sections définies. La FSI est décrite par les équations élargies combinées du coup de bélier et du coup d'acier tandis que le comportement viscoélastique du matériel de la conduite est décrit par un modèle généralisé de Kelvin–Voigt. Les fuites et les blocages sont considérés comme condition de frontière d'extrémité ou intérieure.

Keywords: Air pocket, blockage, cavitation, column separation, fluid–structure interaction, leakage, unsteady friction, viscoelastic behaviour of the pipe-wall, water hammer

Accepted on July 26, 2007/Open for discussion until December 31, 2008.

1 Introduction

1.1 Classical water-hammer

The classical water-hammer equations in terms of piezometric head H and discharge Q are

$$\frac{\partial H}{\partial t} + \frac{a^2}{gA}\frac{\partial Q}{\partial x} = 0 \tag{1}$$

$$\frac{\partial H}{\partial x} + \frac{1}{gA}\frac{\partial Q}{\partial t} + h_f = 0 \tag{2}$$

with the quasi-steady frictional head loss per unit length

$$h_f = f\frac{Q\,|Q|}{2gDA^2} \tag{3}$$

and the wave speed a given by

$$a = \sqrt{\frac{K/\rho}{1+\alpha(K/E)(D/e)}}, \tag{4}$$

where A is the cross-sectional flow area, D is the internal pipe diameter, E is the Young's modulus of elasticity of pipe-wall material, e is the pipe-wall thickness, f is the friction coefficient according to Darcy–Weisbach, g is the gravitational acceleration, K is the bulk modulus of elasticity of liquid, and α is the axial pipe-constraint parameter dependent on Poisson's ratio ν and relative wall thickness e/D. Equations (1) and (2) describe the acoustic behaviour of weakly compressible (elastic) low-Mach-number flows in prismatic pipes of circular cross-section. The pipe-wall is assumed to behave in a linearly elastic manner, and cavitation (including column separation and trapped air pockets), leakages, blockages, and fluid–structure interaction are assumed to be absent. In fact, Eqs (1) and (2) are simplified unsteady pipe flow equations in which the convective transport terms have been neglected. A full derivation of these equations can be found in any textbook pertaining to water hammer (e.g., Wylie and Streeter, 1993; Almeida and Koelle, 1992; Chaudhry, 1987).

The standard procedure to solve Eqs (1) and (2) is the method of characteristics (MOC). This procedure yields water-hammer compatibility equations that are valid along characteristic lines in the distance (x)–time (t) plane. The compatibility equations are numerically integrated to give for the ith computational section at time t (Fig. 1):

— along the C^+ characteristic line ($\Delta x/\Delta t = a$):

$$H_{i,t} - H_{i-1,t-\Delta t} + \frac{a}{gA}((Q_u)_{i,t} - Q_{i-1,t-\Delta t}) + \frac{f\Delta x}{2gDA^2}(Q_u)_{i,t}|Q_{i-1,t-\Delta t}| = 0 \tag{5}$$

— along the C^- characteristic line ($\Delta x/\Delta t = -a$):

$$H_{i,t} - H_{i+1,t-\Delta t} - \frac{a}{gA}(Q_{i,t} - (Q_u)_{i+1,t-\Delta t}) - \frac{f\Delta x}{2gDA^2}Q_{i,t}|(Q_u)_{i+1,t-\Delta t}| = 0. \tag{6}$$

The discharges at the upstream ($(Q_u)_i$) and downstream (Q_i) sides of the ith computational section have been introduced to accommodate the discrete cavity models described in Sec. 3.

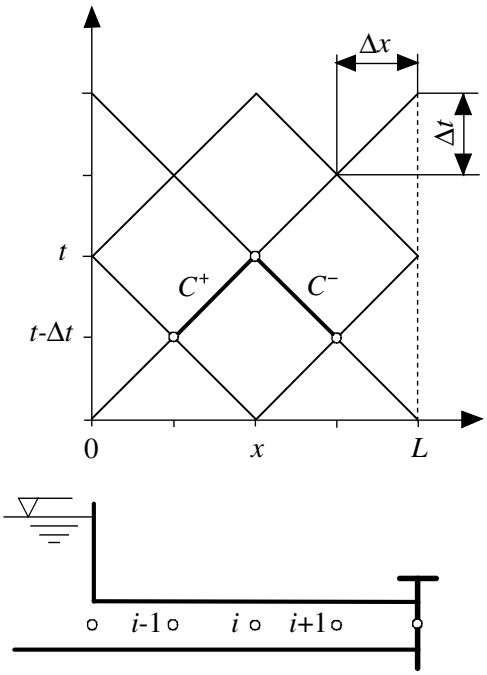

Figure 1 The method of characteristics staggered grid for a reservoir-pipe-valve system

They are identical for the classical water-hammer case, i.e., $Q_u \equiv Q$. Using appropriate boundary and junction conditions, the numerical solution is calculated by time-marching from a given initial condition. It is noted that slightly different computational grids and numerical integration schemes have been used herein, dependent on the computer code used.

1.2 Extended water-hammer

In practice, the conditions in a pipeline system can be far from the idealised situation described by the classical water-hammer equations. Friction, in the classical sense of Eq. (3), gives rise to wave attenuation and line pack. However, occasionally Eq. (3) is not sufficient and more advanced models, referred to as unsteady or frequency-dependent friction, have to be applied. Many other complications may exist in practical situations, such as: air (free and dissolved) in the liquid, cavitation and column-separation (low-pressure phenomena), FSI (if unrestrained pipes move), viscoelastic pipe-wall behaviour (if pipes are made of plastic or if steel pipes deform plastically), and unnoticed leaks, hidden blockages, and thefts at unidentified locations in the system. The modelling of all of these phenomena is the subject of this Part 1, whereas Part 2 concentrates on the effects on the pressure signals. Other complications that may affect the water-hammer waveform include: acoustic radiation, for example in rock-bored tunnels (Fanelli, 1973; Suo and Wylie, 1990), solidified sediment deposit at the pipe walls, and tapered pipes (Adamkowski, 2003). These are beyond the scope of the present paper.

1.3 Aims of the two-part paper

Undesirable water-hammer effects may disturb the overall operation of hydraulic systems and cause damage of fluid machinery,

pipe displacement or even pipe rupture. Calibration and monitoring of hydraulic systems require a detailed knowledge of water-hammer wave attenuation, shape and timing. Engineers should be able to identify parameters that may violate the underlying assumptions in standard water-hammer software packages.

Part 1 presents one-dimensional mathematical models in the framework of the MOC. Numerical models including *all* of the aforementioned phenomena do not exist (to the authors' knowledge) in commercial software. Therefore, the different models presented in Part 1 are made suitable for easy implementation in standard water-hammer codes. Part 2 presents case studies with numerical results showing how a number of important parameters affect water hammer. It is for the first time that these complicating aspects have been brought together in one paper and applied to one water-hammer test system.

2 Unsteady friction

The importance of skin friction in one-dimensional pipe flow models depends on the system considered and on the operating conditions. In the majority of the laboratory water-hammer test rigs unsteady friction dominates over steady friction. Unsteady friction arises from the extra losses caused by the two-dimensional nature of the unsteady velocity profile. In turbulent flow unsteady friction is even a three-dimensional problem. However, fully modelling both the two-dimensional and three-dimensional cases is complicated, computationally expensive and defining the boundary conditions in more complex systems can become difficult. It is therefore desirable to have a model that takes into account higher-dimensional velocity profile behaviour and that still can be efficiently incorporated in a one-dimensional analysis. There are many types of unsteady friction models (Bergant *et al.*, 2001). In this paper, the convolution-based unsteady friction type of model is considered.

2.1 Convolution-based model

The friction head loss can be thought of as comprising a steady part and an unsteady part as follows:

$$h_f = \frac{fQ|Q|}{2gDA^2} + \frac{16\nu}{gD^2A}\left(\frac{\partial Q}{\partial t} * W\right), \tag{7}$$

where ν is the kinematic viscosity, W is the weighting function (in time) and "$*$" denotes convolution. The Darcy–Weisbach relation (3) defines the steady-state component and the unsteady component follows from the convolution of a weighting function (W) with past temporal discharge variations ($\partial Q/\partial t$). Zielke (1968) derived the following approximate time-domain weighting function equation based on analytical solutions obtained for *laminar* flow:

$$W_{\text{app}}(\tau) = \begin{cases} \sum_{j=1}^{6} m_j \tau^{\frac{1}{2}j-1} & \text{for } \tau \le 0.02 \\ \sum_{j=1}^{5} e^{-n_j\tau} & \text{for } \tau > 0.02, \end{cases} \tag{8}$$

where $m_j = \{0.282095, -1.250000, 1.057855, 0.937500, 0.396696, -0.351563\}$, $j = 1, \ldots, 6$, and $n_j = \{26.3744, 70.8493, 135.0198, 218.9216, 322.5544\}$, $j = 1, \ldots, 5$. The weighting function is defined in terms of the dimensionless time $\tau = 4\nu t/D^2$.

Vardy and Brown (1995) used the frozen viscosity assumption to derive a weighting function for *smooth-pipe turbulent* flow. Their approximate weighting function was

$$W_{\text{app}}(\tau) = \frac{A^* e^{-B^*\tau}}{\sqrt{\tau}} \tag{9}$$

where A^* and B^* depend on the Reynolds number ($Re_0 = Q_0 D/(\nu A)$) of the pre-transient flow. Vardy and Brown (2003) defined the coefficients A^* and B^* for smooth-pipe turbulent flow as

$$A^* = \frac{1}{2\sqrt{\pi}} \quad \text{and} \qquad B^* = \frac{Re_0^{\kappa}}{12.86} \quad \text{with} \quad \kappa = \log_{10}(15.29 Re_0^{-0.0567}) \tag{10}$$

These coefficients are accurate in the range $2 \cdot 10^3 < Re_0 < 10^8$.

For fully *rough-pipe turbulent* flow Vardy and Brown (2004) proposed

$$A^* = 0.0103\sqrt{Re_0}\left(\frac{\varepsilon}{D}\right)^{0.39} \quad \text{and} \quad B^* = 0.352 Re_0 \left(\frac{\varepsilon}{D}\right)^{0.41}, \tag{11}$$

where ε/D is the relative pipe-wall roughness. These coefficients are valid for $10^{-6} < \varepsilon/D < 10^{-2}$.

Although convolution-based models for unsteady friction are only approximate and have a finite time-duration of validity, they have resulted in good matches with previous numerical and experimental studies. Vardy and Hwang (1991) showed good matches between a two-dimensional shell model of transient flow and results obtained with the Zielke weighting function. Ghidaoui and Mansour (2002) showed that the Vardy–Brown weighting function produced good matches with experimental data and with the quasi-2D model of Pezzinga (1999) for smooth-pipe turbulent flow.

2.2 Method of characteristics implementation

The finite-difference approximation of the convolution-based unsteady frictional head loss term for the ith computational section in a staggered characteristic grid (Fig. 1) is

$$(h_f)_{i,t} = \frac{f_0 Q_{i,t}|Q_{i,t}|}{2gDA^2} + \frac{16\nu}{gD^2A} \times \sum_{j=1,3,5,\ldots}^{M} (Q_{i,t-j\Delta t+\Delta t} - Q_{i,t-j\Delta t-\Delta t})\, W_{\text{app}}(j\Delta t), \tag{12}$$

where $M = t/\Delta t - 1$. A first-order approximation term $f\Delta x/(2gDA^2)Q_{t-\Delta t}|Q_{t-\Delta t}|$ is used in Eqs (5) and (6) (Bergant *et al.* 2001). Equation (12), called the full-convolution scheme and first implemented by Zielke (1968), is computationally expensive. Trikha (1975) and Kagawa *et al.* (1983) improved the computational efficiency by further approximating Zielke's weighting function. Ghidaoui and Mansour (2002) presented an

efficient implementation of the Vardy and Brown (1995) weighting function. Vítkovský *et al.* (2004) developed computationally efficient and accurate approximations of both the Zielke and any of the Vardy–Brown weighting functions.

3 Cavitation

Low pressures during transient events in pipelines often result in cavitating flow. Cavitation significantly changes the pressure waveform and the water-hammer equations developed for pure liquid flow are not valid anymore. Two basic types of transient cavitating flow can be distinguished: one-component two-phase transient flow (vaporous cavitation; liquid column separation) and two-component two-phase transient flow (gaseous cavitation; free gas in liquid flow). A historical review of the subject is given by Bergant *et al.* (2006).

3.1 Vaporous cavitation and DVCM

Vaporous cavitation (including column separation) occurs in pipelines when the liquid pressure suddenly drops to the vapour pressure. Cavitation may occur as a local vapour cavity (large void fraction, often leading to a column separation) and/or as distributed vaporous cavitation (small void fractions). A large local (discrete) vapour cavity may form at a boundary (shut-off gate or valve, draft tube of a water turbine), at a high point or knee, or at any place in a pipe (intermediate cavity) when two low-pressure waves meet (Bergant and Simpson, 1999). Distributed vaporous cavitation occurs when a rarefaction wave drops the pressure to vapour pressure in an extended length of pipe. Pressure waves do not propagate through an established mixture of liquid and vapour bubbles, because the pressure simply stays constant; this inability distinguishes vaporous cavitation from gaseous cavitation. Both the inertia-driven collapse of a large vapour cavity and the movement of a pressure wave front into a vaporous cavitation zone make the vapour condense back to liquid. A number of vaporous cavitation models have been developed (Wylie and Streeter, 1993; Simpson and Bergant, 1994; Bergant and Simpson, 1999) including discrete cavity and interface models.

The discrete vapour cavity model (DVCM) is widely used in standard water-hammer software packages. It allows vapour cavities to form at computational sections in the MOC when the pressure drops to the liquid's vapour pressure. Pure liquid with a constant wave speed a is assumed to occupy the reach in between two computational sections. The discrete vapour cavity is described by Eqs (5) and (6), with $Q_u \neq Q$ and H set to the vapour head, and its volume $\forall_v$ is governed by the continuity equation:

$$\forall_v = \int_{t_{in}}^{t} (Q - Q_u)dt, \tag{13}$$

which is numerically approximated by (Fig. 1):

$$(\forall_v)_{i,t} = (\forall_v)_{i,t-2\Delta t} + \{(1-\psi)[Q_{i,t-2\Delta t} - (Q_u)_{i,t-2\Delta t}] + \psi[Q_{i,t} - (Q_u)_{i,t}]\}2\Delta t \tag{14}$$

in which t_{in} is the time of cavitation inception and ψ is the weighting factor. The weighting factor ψ is taken between 0.5 and 1.0 to obtain numerical stability. The cavity collapses when its calculated volume becomes less than zero. The liquid phase is re-established and the water-hammer solution using Eqs (5) and (6) (with $Q \equiv Q_u$) is valid again. The DVCM may generate unrealistic pressure pulses (spikes) due to the collapse of multi-cavities, but the model gives reasonably accurate results when the number of reaches is restricted. It is recommended that the maximum volume of discrete cavities at sections is less than 10% of the reach volume (Simpson and Bergant, 1994).

3.2 Gaseous cavitation and DGCM

Gaseous cavitation occurs in fluid flows when free gas is either distributed throughout the liquid (small void fractions) or trapped at distinct positions along the pipe and at boundaries (larger void fractions). Trapped gas pockets are known to cause severe operational problems in piping systems. During low-pressure transients the gas bubbles grow and dissolved gas may come out of solution (gas release). Transient gaseous cavitation is associated with wave dispersion and shock waves. The wave speed in a gas–liquid mixture is pressure dependent and generally it is significantly lower than the liquid wave speed a. Gas release takes several seconds whereas vapour formation takes only a few milliseconds (for water at room temperature). The effect of gas release during transients is important in long pipelines for which the wave reflection time is at least in the order of several seconds. Empirical methods for describing the amount of gas release were, amongst others, developed by Zielke and Perko (1985).

Transient flow of a homogeneous gas–liquid mixture with a low gas fraction may be described by the classical water-hammer equations (1) and (2) in which the liquid wave speed a is replaced by the wave speed a_m (Wylie, 1984):

$$a_m = \sqrt{\frac{a^2}{1 + \frac{\alpha_g a^2}{g(H-z-H_v)}}}, \tag{15}$$

where α_g is the gas void fraction, z is the pipeline elevation, and H_v is the gauge vapour head. The pressure-head dependent wave speed a_m makes the system of equations highly nonlinear. A number of numerical schemes including the MOC have been used for solving the problem of the gas–liquid mixture (Wylie, 1980; Chaudhry *et al.*, 1990; Wylie and Streeter, 1993). These methods are complex and cannot be easily incorporated into a standard water-hammer code. Alternatively, the distributed free gas can be lumped at computational sections leading to the discrete gas cavity model (DGCM).

The DGCM allows gas cavities to exist at computational sections. As in the DVCM, pure liquid with a constant wave speed a is assumed to occupy the computational reaches in between. The discrete gas cavity is described by the water-hammer compatibility equations (5) and (6), the continuity equation for the gas cavity volume (14) (index g replaces v), and the ideal gas equation (assuming isothermal conditions):

$$(H - z - H_v)\forall_g = (H_0 - z - H_v)\forall_{g0} \tag{16}$$

in which $\forall_g$ is the gas volume and subscript "0" indicates the initial situation. The treatment of gas release in the DGCM using the method proposed by Zielke and Perko (1985) is straightforward (Barbero and Ciaponi, 1991). Naturally, DGCM can be used to model a single air pocket (air pocket volume to be less than 10% of the reach volume). In addition, the DGCM can be successfully used for the simulation of vaporous cavitation by utilizing a low initial gas void fraction ($\alpha_{g0} = \forall_{g0}/\forall_{\text{reach}} \leq 10^{-7}$) at all computational sections (Wylie, 1984; Simpson and Bergant, 1994).

4 Fluid–structure interaction

The quality of results obtained with the classical water-hammer Eqs (1) and (2) depends highly on a good estimate of the magnitude of the pressure wave speed a. Consequently, it is best to determine a directly from measurements. Theoretical estimates of a are usually valid for thin-walled pipes with either zero axial stress ($\alpha = 0$) or zero axial strain ($\alpha = 1 - \nu^2$). If non-zero dynamic axial stresses and strains in the pipe-wall are taken into account, the following *extended water-hammer equations* are obtained

$$\frac{\partial H}{\partial t} + \frac{a^2}{gA}\frac{\partial Q}{\partial x} = 2\nu\frac{a^2}{g}\frac{\partial \dot{u}_x}{\partial x} \tag{17}$$

$$\frac{\partial H}{\partial x} + \frac{1}{gA}\frac{\partial Q}{\partial t} + \frac{fQ_{\text{rel}}|Q_{\text{rel}}|}{2gDA^2} = 0, \tag{18}$$

where a is defined by Eq. (4) with $\alpha = 1 - \nu^2$. The right-hand term in Eq. (17) is the time derivative of the axial strain, which is equal to the spatial derivative of the axial pipe-wall velocity $\dot{u}_x$, multiplied by two times Poisson's ratio ν and a^2/g. To determine the pipe velocity $\dot{u}_x$, two additional equations have to be solved. These may be named *extended steel-hammer equations*, because they are mathematically equivalent to the Eqs (17) and (18),

$$\frac{\partial \sigma_x}{\partial t} - \rho_s a_s^2\frac{\partial \dot{u}_x}{\partial x} = \nu\rho g\frac{D}{2e}\frac{\partial H}{\partial t} \tag{19}$$

$$\frac{\partial \sigma_x}{\partial x} - \rho_s\frac{\partial \dot{u}_x}{\partial t} + \frac{f\rho Q_{rel}|Q_{rel}|}{8eA^2} - \rho_s g\sin\theta = 0 \tag{20}$$

in which σ_x is the axial stress, ρ_s is the mass density of the pipe-wall material, $a_s = \sqrt{(E/\rho_s)}$ is the stress wave speed, and Q_{rel} is the discharge relative to the moving pipe-wall. The MOC transforms the four coupled Eqs (17)–(20) to compatibility equations which, disregarding skin friction and gravity, and in terms of pressures (p) and fluid velocities (V) to see the mathematical analogy with stresses and structural velocities, read as follows:

$$\frac{dp}{dt} \pm \rho\tilde{a}\frac{dV}{dt} + G_f\left\{\frac{d\sigma_x}{dt} \mp \rho_s\tilde{a}\frac{d\dot{u}_x}{dt}\right\} = 0 \tag{21}$$

$$\frac{d\sigma_x}{dt} \mp \rho_s\tilde{a}_s\frac{d\dot{u}_x}{dt} + G_s\left\{\frac{dp}{dt} \pm \rho\tilde{a}_s\frac{dV}{dt}\right\} = 0. \tag{22}$$

Equations (21) and (22) are valid along characteristic lines with $dx/dt = \pm\tilde{a}$ and $dx/dt = \pm\tilde{a}_s$, respectively, and the *Poisson coupling* factors G_f and G_s are

$$G_f = -2\nu\frac{\rho}{\rho_s}\left[\left(\frac{a_s}{\tilde{a}}\right)^2 - 1\right]^{-1} \quad \text{and}$$

$$G_s = \nu\frac{D}{2e}\left[\left(\frac{\tilde{a}_s}{a}\right)^2 - 1\right]^{-1}. \tag{23}$$

The modified wave speeds $\tilde{a}$ and $\tilde{a}_s$ follow directly from the characteristic equation of the coupled system of Eqs (17)–(20). In water-filled steel pipes, the modified wave speeds $\tilde{a}$ and $\tilde{a}_s$ are slightly different from a and a_s (Stuckenbruck *et al.*, 1985; Leslie and Tijsseling, 1999): $\tilde{a} < a$ because of added (pipe) mass and $\tilde{a}_s > a_s$ because of added (liquid) stiffness. Each jump in pressure travelling at speed $\tilde{a}$ is now accompanied with a jump in axial pipe stress according to (Tijsseling, 1993)

$$\Delta\sigma_x = -G_s\Delta p. \tag{24}$$

Similarly, each jump in axial stress travelling at speed $\tilde{a}_s$ is accompanied with a jump in pressure (precursor) according to

$$\Delta p = -G_f\Delta\sigma_x. \tag{25}$$

The relations (24) and (25), together with the definitions (23), say something about the importance of *distributed* FSI.

Local FSI occurs at valves, orifices, expansions, contractions, elbows, bends and branches, noting that under severe transients all these pipe components will vibrate to a certain extent. The dynamic interaction of a local component with flow unsteadiness is called *junction coupling*. The simplest example is the closed free end where fluid and structural velocities, and pressures and stresses, are proportional to each other

$$V = \dot{u}_x \quad \text{and} \quad Ap = A_s\sigma_x. \tag{26}$$

Herein, FSI is related to axial modes of pipe vibration without wavefront distortion (Tijsseling *et al.*, 2006). In general, pipe flexure and pipe torsion must be taken into consideration because of their coupling to axial modes. More information on the subject can be found in reviews by Wiggert (1996), Tijsseling (1996), and Wiggert and Tijsseling (2001).

5 Viscoelastic behaviour of the pipe-wall

Plastic pipes are being increasingly used in water supply systems due to their high resistant properties (mechanical, chemical, temperature, and abrasion) and low price. The viscoelastic behaviour of plastic pipes influences the water-hammer event by attenuating the pressure fluctuations and by increasing the dispersion of the travelling wave. Sections of viscoelastic pipe have been used to suppress dangerously large transients due to the high dispersion and damping exhibited by the pipe section's viscoelasticity (Pezzinga and Scandura, 1995). An approach based on the mechanical principle associated with viscoelasticity, in which strain can be decomposed into instantaneous elastic strain and retarded viscoelastic strain, is used herein. The elastic strain component is included in the wave speed, whereas the viscoelastic strain component is included as an additional term in the continuity equation (Rieutord and Blanchard, 1979; Gally *et al.*, 1979).

5.1 Linear viscoelastic model

Plastic pipes have a different constitutive behaviour compared to metal and concrete pipes. When subjected to an instantaneous stress σ, polymers do not respond according to Hooke's law. Polymers have an instantaneous elastic response and a retarded viscous response. Consequently, the total strain ε can be decomposed into an elastic component ε_e and a retarded component ε_{ret} as

$$\varepsilon = \varepsilon_e + \varepsilon_{\text{ret}}. \tag{27}$$

For small strains, a combination of stresses that act independently results in strains that can be added linearly. The total strain ε generated by a continuous application of stress σ is

$$\varepsilon = \sigma J_0 + \sigma * \frac{\partial J}{\partial t}, \tag{28}$$

where J_0 is the instantaneous creep-compliance and J is the creep-compliance function of time t, and "$*$" denotes convolution. For linearly elastic materials, the constant creep-compliance J_0 is equal to the inverse of Young's modulus of elasticity, i.e., $J_0 = 1/E_0$. For a material that is homogeneous and isotropic, and for small strains, Poisson's ratio ν is approximately constant. The circumferential pipe stress σ_φ is related to the gauge pressure by $\sigma_\varphi = pD/(2e)$. The circumferential strain defined by $\varepsilon_\varphi = 2u_r/D$, where u_r is the radial displacement of the pipe wall, is related to the pipe stresses by $\varepsilon_\varphi = (\sigma_\varphi - \nu\sigma_x)/E$. The linear viscoelastic behaviour of the pipe wall for small strains and no dynamic FSI effects may now be approximated as (Güney 1983)

$$\varepsilon_\varphi(t) = \frac{\alpha D}{2e}[p(t) - p_0]J_0 + \frac{\alpha D}{2e}\int_0^t [p(t-t^*) - p_0]\frac{\partial J(t^*)}{\partial t^*}dt^*. \tag{29}$$

The subscript "0" corresponds to steady-state conditions. The first term on the right-hand side of Eq. (29) corresponds to the elastic circumferential strain $(\varepsilon_\varphi)_e$ and the second term to the retarded circumferential strain $(\varepsilon_\varphi)_{\text{ret}}$. The creep-compliance function $J(t)$, which describes the viscoelastic behaviour of the pipe material, can be determined experimentally using a mechanical test or calibrated (tuned) on collected transient data (Covas *et al.*, 2004, 2005). A mechanical model of the generalised viscoelastic solid is typically used to describe the creep function (Aklonis *et al.*, 1972), for example a generalised Kelvin–Voigt model consisting of N parallel spring and dashpot elements in series,

$$J(t) = J_0 + \sum_{k=1}^{N} J_k(1 - e^{-t/\tau_k}), \tag{30}$$

where the stiffness of each spring is $E_k = 1/J_k$, the viscosity of each dashpot is η_k, and the associated retardation time is $\tau_k = \eta_k/E_k$. The creep-compliance function for a material is dependent on temperature, stress, age, and orientation as a result of the manufacturing process (Lai and Bakker, 1995). These effects are not included in Eq. (30).

When the viscoelastic model equation (29), with $p = \rho g H - x\sin\theta$, is incorporated in the water-hammer equations (1) and (2), the equation that represents the conservation of mass becomes

$$\frac{\partial H}{\partial t} + \frac{a^2}{gA}\frac{\partial Q}{\partial x} + \frac{2a^2}{g}\frac{\partial(\varepsilon_\varphi)_{\text{ret}}}{\partial t} = 0. \tag{31}$$

The influence of the elastic strain $(\varepsilon_\varphi)_e$ is already included in the liquid wave speed a (Eq. (4)). The viscoelastic model does not change the equation of motion Eq. (2).

5.2 Method of characteristics implementation

After applying the MOC to the extended water-hammer equations (31) and (2), the corresponding compatibility equations become

$$\frac{dH}{dt} \pm \frac{a}{gA}\frac{dQ}{dt} + \frac{2a^2}{g}\frac{\partial(\varepsilon_\varphi)_{\text{ret}}}{\partial t} \pm a h_f = 0 \quad \text{along } \frac{dx}{dt} = \pm a, \tag{32}$$

where the partial derivative of the retarded strain in the pipe-wall with respect to time is

$$\frac{\partial(\varepsilon_\varphi)_{\text{ret}}}{\partial t}(x,t) = \frac{\alpha D}{2e}\rho g\int_0^t \frac{\partial H(x,t-t^*)}{\partial t}\frac{\partial J(t^*)}{\partial t}dt^*. \tag{33}$$

The integration in the above equation is performed numerically with the trapezoidal rule so that the retarded strain term for the ith computational section in the characteristic grid (Fig. 1) is

$$\left(\frac{\partial(\varepsilon_\varphi)_{\text{ret}}}{\partial t}\right)_{i,t} = \frac{\alpha D}{2e}\rho g \times \sum_{j=1,3,5}^{M}(H_{i,t-j\Delta t+\Delta t} - H_{i,t-j\Delta t-\Delta t})\frac{\partial J}{\partial t}(j\Delta t), \tag{34}$$

where $M = t/\Delta t - 1$. This scheme, called the full-convolution scheme, is computationally expensive which can be prohibitive to its use. An efficient implementation is similar to that of the convolution-based unsteady friction term in Sec. 2.2. Gally *et al.* (1979) outlined an efficient recursive formulation using the Kelvin–Voigt approximation of the creep-compliance function. Numerical schemes used for the calculation of the strain $(\varepsilon_\varphi)_{\text{ret}}$ and its time derivative can be found in Covas *et al.* (2004, 2005).

6 Discrete leakage and blockage

Leaks and blockages represent common faults that pipeline systems can experience during their design lifetime. In many cases transients measured in the field show significantly more damping than what is predicted by models (including unsteady friction). In some cases this additional damping is caused by unknown faults such as leaks and blockages. These are complementary phenomena; for example, a leak represents a flow loss with no head loss, whereas a blockage represents a head loss with no flow

loss. Discrete leaks and blockages are modelled using the orifice equation

$$Q_{\mathrm{Or}} = C_d A_{\mathrm{Or}} \sqrt{2g\Delta H_{\mathrm{Or}}}, \tag{35}$$

where C_d is the discharge coefficient and subscript "Or" relates to orifice. For both leaks and blockages, Eq. (35) is implemented in the MOC as an internal boundary condition.

Discrete leaks are treated as an off-line orifice. The relationship that relates the upstream flow Q_u to the downstream flow Q is

$$Q_u - Q - C_d A_{\mathrm{Or}} \sqrt{2g(H_{\mathrm{Or}} - h_{\mathrm{OUT}} - z)} = 0, \tag{36}$$

where h_{OUT} is the pressure head outside the leak. In most cases the outside head is the atmospheric pressure head and assumed zero. Equations (5), (6), and (36) combine to a quadratic equation in H_{Or} that is solved exactly using the quadratic formula. Once H_{Or} is determined, the upstream and downstream flows are calculated using the positive and negative compatibility equations (5) and (6), respectively. Care must be taken to account for the case when the pressure inside the pipe becomes less than the outside pressure. In that case, Eq. (36) is rewritten assuming that the leak works in reverse, thus injecting fluid into the pipe. For real leaks, it is unlikely that the orifice equation will perfectly describe their behaviour. Real leaks come in a variety of sizes and shapes which results in deviations from the classical orifice relationship (35). In many cases a power law can be used for modelling the discharge-head loss relationship; however, the details of the leak are usually unknown and the orifice relation is sufficient.

Discrete blockages are treated as an in-line orifice. The upstream head H_u and downstream head H are related to the flow through the blockage by

$$Q_{\mathrm{Or}}|Q_{\mathrm{Or}}| - 2g(C_d A_{\mathrm{Or}})^2 (H_u - H) = 0. \tag{37}$$

Equations (5), with H set to H_u, (6) and (37) combine to a quadratic equation in Q_{Or} and can be solved using the quadratic formula, where care must be taken again when the flow through the orifice reverses. The orifice equation represents the simplest model of a blockage which in most cases will adequately approximate a blockage of any shape and length. Additionally, for certain pipe flows a blockage can cause additional delays in the transient response due to inertial lengths associated with the submerged jet created by the blockage (Prenner, 1997).

7 Conclusions

State-of-the-art mathematical models have been presented that describe unsteady friction, cavitation (including column separation and trapped air pockets), fluid–structure interaction, pipe-wall viscoelasticity, and leakages and blockages in transient pipe flow. The models are based on the method of characteristics (MOC) such that they can easily be incorporated in conventional water-hammer software. Trapped air pockets, leakages and blockages are simply modelled as (internal) boundary conditions. Cavitation is implicitly also modelled by (internal) boundary conditions, but in addition cavity volumes have to be kept track of. Unsteady friction and wall viscoelasticity are modelled by adding one term to the momentum and continuity equation, respectively. Flow and pressure history are needed in the calculation of this added term, because it is a convolution. Fluid–structure interaction is modelled by one additional term in the continuity equation, but to calculate this term two new equations are needed which describe the axial transients in the pipe wall. Fortunately, the new equations can be solved by the MOC, because they are analogous to the classical water-hammer equations. Part 2 of the two-part paper shows a selection of results obtained with the presented models.

Notation

A = Cross-sectional flow area
A_{Or} = Cross-sectional orifice area
A_s = Cross-sectional pipe-wall area
a = Liquid wave speed
a_m = Gas–liquid mixture wave speed
a_s = Solid wave speed
$\tilde{a}$ = FSI-modified wave speed
A^*, B^*, κ = Vardy–Brown weighting function coefficients
C_d = Orifice discharge coefficient
D = Internal pipe diameter
E = Young's modulus of elasticity of pipe-wall material; spring stiffness
e = Pipe-wall thickness
f = Darcy–Weisbach friction factor
G_f, G_s = FSI Poisson coupling factors
g = Gravitational acceleration
H = Piezometric head; downstream head in Eq. (37)
H_v = Gauge vapour head
h_f = Frictional head loss per unit length
h_{OUT} = Pressure head outside the leak
J = Creep-compliance function
J_k = Kelvin–Voigt model parameter
J_0 = Instantaneous creep-compliance
K = Bulk modulus of elasticity of liquid
m_j, n_j = Zielke weighting function coefficients
p = Pressure
Q = Discharge (flow rate); downstream-end discharge at node
Re = Reynolds number ($Re = VD/\nu$)
t, t^* = Time
t_{in} = Time of cavitation inception
u = Pipe-wall displacement
$\dot{u}$ = Pipe-wall velocity
V = Cross-sectionally averaged flow velocity
$\forall$ = Discrete cavity volume
W = Weighting function for convolution-based unsteady friction model
x = Axial distance
z = Pipeline elevation
α = Parameter dependent on the axial pipe constraints
α_g = Gas void fraction
ΔH_{Or} = Head loss across orifice

Δp = Jump in pressure
Δt = MOC time step
Δx = MOC space step
$\Delta\sigma_x$ = Jump in axial stress
ε = Total strain; pipe-wall roughness
ε_e = Elastic strain component
ε_{ret} = Retarded strain component
ε_φ = Total circumferential strain
η_k = Dashpot viscosity
θ = Pipe slope
ν = Kinematic viscosity; Poisson's ratio
ρ = Mass density of liquid
ρ_s = Mass density of the pipe-wall material
σ = Stress
σ_x = Axial stress
σ_φ = Circumferential stress
τ = Dimensionless time ($\tau = 4\nu t/D^2$)
τ_k = Retardation time in Kelvin–Voigt model
ψ = Weighting factor

Subscripts

app = Approximate
e = Elastic
g = Gas
i = Node number
Or = Orifice
r = Radial direction
rel = Relative to pipe-wall
ret = Viscoelastic retardation
s = Structure, solid, pipe
u = Upstream side of computational section
v = Vapour
x = Axial direction
0 = Steady-state (initial) conditions

Abbreviations

DGCM = Discrete gas cavity model
DVCM = Discrete vapour cavity model
FSI = Fluid–structure interaction
MOC = Method of characteristics.

Acknowledgement and disclaimer

The Surge-Net project is supported by funding under the European Commission's Fifth Framework "Growth" Programme via Thematic Network "Surge-Net" contract reference: G1RT-CT-2002-05069. The authors of this paper are solely responsible for the content and it does not represent the opinion of the Commission. The Commission is not responsible for any use that might be made of data herein.

References

Adamkowski, A. (2003). Analysis of transient flow in pipes with expanding or contracting sections. *J. Fluids Eng. ASME* 125(4), 716–722.

Aklonis, J.J., MacNight, W.J., Shen, M. (1972). *Introduction to Polymer Viscoelasticity*. Wiley-Interscience, John Wiley & Sons, Inc., New York, USA.

Almeida, A.B., Koelle, E. (1992). *Fluid Transients in Pipe Networks*. Computational Mechanics Publications, Ashurst, United Kingdom.

Barbero, G., Ciaponi, C. (1991). Experimental validation of a discrete free gas model for numerical simulation of hydraulic transients with cavitation. *Proceedings of the International Meeting on Hydraulic Transients with Column Separation, 9th Round Table*, IAHR, Valencia, Spain, 17–33.

Bergant, A., Simpson, A.R. (1999). Pipeline column separation flow regimes. *J. Hydraul. Eng. ASCE* 125(8), 835–848.

Bergant, A., Simpson, A.R., Vítkovský, J. (2001). Developments in unsteady pipe flow friction modelling. *J. Hydraul. Res. IAHR* 39(3), 249–257.

Bergant, A., Simpson, A.R., Tijsseling, A.S. (2006). Water hammer with column separation: A historical review. *J. Fluids* and *Struct.* 22(2), 135–171.

Chaudhry, M.H. (1987). *Applied Hydraulic Transients*, 2nd edn., Van Nostrand Reinhold, New York, USA.

Chaudhry, M.H., Bhallamudi, S.M., Martin, C.S., Nagash, M. (1990). Analysis of transient pressures in bubbly, homogeneous, gas-liquid mixtures. *J. Fluids Eng. ASME* 112(2), 225–231.

Covas, D., Stoianov, I., Mano, J.F., Ramos, H., Graham, N., Maksimovic, C. (2004). The dynamic effect of pipe-wall viscoelasticity in hydraulic transients. Part I—Experimental analysis and creep characterisation. *J. Hydraul. Res. IAHR* 42(5), 516–530.

Covas, D., Stoianov, I., Mano, J.F., Ramos, H., Graham, N., Maksimovic, C. (2005). The dynamic effect of pipe-wall viscoelasticity in hydraulic transients. Part II—Model development, calibration and verification. *J. Hydraul. Res. IAHR* 43(1), 56–70.

Fanelli, M. (1973). Hydraulic resonance in rock-bored penstocks. *Water Power* 25(9), 342–346.

Gally, M., Güney, M., Rieutord, E. (1979). An investigation of pressure transients in viscoelastic pipes". *J. Fluids Eng. ASME* 101(4), 495–499.

Ghidaoui, M.S., Mansour, S. (2002). Efficient treatment of Vardy-Brown unsteady shear in pipe transients. *J. Hydraul. Eng. ASCE* 128(1), 102–112.

Güney, M.S. (1983). Waterhammer in viscoelastic pipes where cross-section parameters are time dependent. *Proceedings of the 4th International Conference on Pressure Surges*, BHRA, Bath, United Kingdom, 189–204.

Kagawa, T., Lee, I., Kitagawa, A., Takenaka, T. (1983). High speed and accurate computing method of frequency-dependent friction in laminar pipe flow for characteristics method. *Trans. Jpn. Soc. Mech. Eng.* 49(447), 2638–2644 (in Japanese).

Lai, J., Bakker, A. (1995). Analysis of the non-linear creep of high-density polyethylene. *Polymer* 36(1), 93–99.

Leslie, D.J., Tijsseling, A.S. (1999). Wave speeds and phase velocities in liquid-filled pipes. *Proceedings of the 9th International Meeting of the IAHR Work Group on the Behaviour of Hydraulic Machinery under Steady Oscillatory Conditions*, Brno, Czech Republic, Paper E1.

Pezzinga, G., Scandura, P. (1995). Unsteady flow in installations with polymeric additional pipe. *J. Hydraul. Eng. ASCE* 121(11), 802–811.

Pezzinga, G. (1999). Quasi-2d model for unsteady flow in pipe networks. *J. Hydraul. Eng. ASCE* 125(7), 676–685.

Prenner, R. (1997). Das Widerstandsverhalten von Kreisblenden in Druckstoßsystemen. Ph.D. Thesis, Technical University Vienna, Vienna, Austria (in German).

Rieutord, E., Blanchard, A. (1979). Ecoulement non-permanent en conduite viscoelastique—coup de bélier. *J. Hydraul. Res. IAHR* 17(1), 217–229 (in French).

Simpson, A.R., Bergant, A. (1994). Numerical comparison of pipe-column-separation models. *J. Hydraul. Eng. ASCE* 120(3), 361–377.

Stuckenbruck, S., Wiggert, D.C., Otwell, R.S. (1985). The influence of pipe motion on acoustic wave propagation. *J. Fluids Eng. ASME* 107(4), 518–522.

Suo, L., Wylie, E.B. (1990). Hydraulic transients in rock-bored tunnels. *J. Hydraul. Eng. ASCE* 116(2), 196–210.

Tijsseling, A.S. (1993). Fluid-structure interaction in case of waterhammer with cavitation. Ph.D. Thesis, Delft University of Technology, Faculty of Civil Engineering, Delft, The Netherlands. Available from: www.darenet.nl/en/page/language.view/search.page.

Tijsseling, A.S. (1996). Fluid-structure interaction in liquid-filled pipe systems: A review. *J. Fluids Struct.* 10(2), 109–146.

Tijsseling, A.S., Lambert, M.F., Simpson, A.R., Stephens, M.L., Vítkovský, J.P., Bergant, A. (2006). Wave front dispersion due to fluid-structure interaction in long liquid-filled pipelines. *Proceedings of the 23rd IAHR Symposium on Hydraulic Machinery and Systems,* Yokohama, Japan, Paper 143.

Trikha, A.K. (1975). An efficient method for simulating frequency-dependent friction in transient liquid flow. *J. Fluids Eng. ASME* 97(1), 97–105.

Vardy, A.E., Hwang, K.-L. (1991). A characteristics model of transient friction in pipes. *J. Hydraul. Res. IAHR* 29(5), 669–684.

Vardy, A.E., Brown, J.M. (1995). Transient, turbulent, smooth pipe friction. *J. Hydraul. Res. IAHR* 33(4), 435–456.

Vardy, A.E., Brown, J.M.B. (2003). Transient turbulent friction in smooth pipe flows. *J. Sound Vibration* 259(5), 1011–1036.

Vardy, A.E., Brown, J.M.B. (2004). Transient turbulent friction in fully-rough pipe flows. *J. Sound Vibration* 270(1–2), 233–257.

Vítkovský, J., Stephens, M., Bergant, A., Lambert, M., Simpson, A. (2004). Efficient and accurate calculation of zielke and vardy-brown unsteady friction in pipe transients. *Proceedings of the 9th International Conference on Pressure Surges*, BHR Group, Chester, United Kingdom, II, 405–419.

Wiggert, D.C. (1996). Fluid transients in flexible piping systems (a perspective on recent developments). *Proceedings of the 18th IAHR Symposium on Hydraulic Machinery and Cavitation,* Valencia, Spain, 58–67.

Wiggert, D.C., Tijsseling, A.S. (2001). Fluid transients and fluid-structure interaction in flexible liquid-filled piping. *ASME Appl. Mech. Rev.* 54(5), 455–481.

Wylie, E.B. (1980). Free air in liquid transient flow. *Proceedings of the 3rd International Conference on Pressure Surges*, BHRA, Canterbury, United Kingdom, 27–42.

Wylie, E.B. (1984). Simulation of vaporous and gaseous cavitation. *J. Fluids Eng. ASME* 106(3), 307–311.

Wylie, E.B., Streeter, V.L. (1993). *Fluid Transients in Systems*. Prentice Hall, Englewood Cliffs, USA.

Zielke, W. (1968). Frequency-dependent friction in transient pipe flow. *J. Basic Eng. ASME* 90(1), 109–115.

Zielke, W., Perko, H.D. (1985). Unterdruckerscheinungen und druckstoßberechnung. *3R Int.* 24(7), 348–355 (in German).